Preventing Kinetic Roughening in Physical Vapor-Phase-Deposited Films

E. Vasco,[1,*] C. Polop,[2] and J. L. Sacedón[1]

[1]*Instituto de Ciencia de Materiales de Madrid, Consejo Superior de Investigaciones Científicas, 28049 Madrid, Spain*
[2]*Dept. Física de la Materia Condensada, Universidad Autónoma de Madrid, 28049 Madrid, Spain*

(Received 31 July 2007; published 8 January 2008)

The growth kinetics of the mostly used physical vapor-phase deposition techniques —molecular beam epitaxy, sputtering, flash evaporation, and pulsed laser deposition—is investigated by rate equations with the aim of testing their suitability for the preparation of ultraflat ultrathin films. The techniques are studied in regard to the roughness and morphology during early stages of growth. We demonstrate that pulsed laser deposition is the best technique for preparing the flattest films due to two key features [use of (i) a supersaturated pulsed flux of (ii) hyperthermal species] that promote a kinetically limited Ostwald ripening mechanism.

DOI: 10.1103/PhysRevLett.100.016102 PACS numbers: 81.15.Aa, 68.55.A−, 81.15.Kk

Current thin-film technologies, in particular, those based on physical vapor-phase deposition (PVD) techniques, present severe limitations for the preparation of ultrathin films with homogeneous thicknesses (d) of only a few atomic monolayers (ML). At this thickness scale ($d \leq 2$ nm), the film roughness (ω), which is mostly determined by the growth kinetics of the deposition technique used, is of the same order of magnitude as the film thickness. This produces a large dispersion of behaviors for thickness-dependent properties. For example, in spintronic devices (e.g., magnetic tunneling junctions) based on spin-polarized tunneling currents through an ultrathin barrier layer, a barrier thickness dispersion of $\delta d/d = 20\%$ [e.g., $d \pm \delta d = 2.0 \pm 0.4$ nm-thick MgO barrier, $\omega \sim 0.28$ nm ($\omega \sim 1.3$ ML), stacked between CoFeB layers] [1] gives rise to a dispersion of tunneling current densities [$J(V) \sim e^{-d\sqrt{\phi - V/2}}$] of $10^3\%$. This means that smaller variations of the tunneling magnetoresistance ratio (TMR) like the best ones reported so far [1] (TMR $\sim$ 200%–400%) are locally indistinguishable from the contribution of the thickness distribution to the tunneling current. Consequently, the reliability of such tunneling junctions to be used in devices is compromised being comparable only TMR responses for junctions with barrier layers having similar thickness distributions. Therefore, the preparation of atomically flat layers (implying the lowest ω) is a technological issue of prime importance to implement reliable ultra-thin-film-based devices.

The inherent roughness (termed kinetic roughening) results from kinetic limitations on the relaxation of random fluctuations in the incoming flux during thin-film growth. The formation of monatomic steps with step-edge barriers hindering interlayer mass exchange is a commonly encountered surface kinetic limitation. In this case, an increase in the growth temperature to promote step-edge barrier crossing and/or atomic exchange with underlying terraces induces a converse effect: an entropy-controlled transition (thermal roughening) [2] to rough surfaces with an increasing density of steps and faceting phenomena. Consequently, alternative surface flattening routes to heating must be explored in the preparation of ultrathin films by PVD.

In the present study, we use mean-field rate-equations to investigate the suitability of four distinctive PVD techniques—molecular beam epitaxy (MBE), sputtering (SP), flash evaporation (FE; a type of pulsed thermal evaporation), and pulsed laser deposition (PLD)—for preparing ultraflat films compatible with ultra-thin-film-based applications. Particularly, we examine the evolution of inherent roughnesses during early stages of growth (prior to ML completion) considering three ranges of kinetic energy (E^{kin})—thermal, hyperthermal, and energetic—for the incident species. The simulation results are discussed in terms of the balance between two complementary mechanisms: (i) coarsening due to the aggregation of small species and island coalescence, and (ii) coarsening by kinetically limited Ostwald ripening.

To address the atomistic scenario of epitaxial growth from the vapor phase on a singular surface (terrace width $\gg$ diffusion length, λ), we use a modified rate equation approach with the following generalized form [3]:

$$\begin{aligned}\frac{\partial \rho_n^k}{\partial t} = {} & m^{k-1}\rho_m^{k-1}F[A_{n-1}\rho_{n-1}^k - A_n\rho_n^k] \\ & + \sum_{i=1}^{n-1}[D_i\sigma_{n-i} + D_{n-i}\sigma_i]\rho_i^k\rho_{n-i}^k \\ & - \sum_{i=1}^{n_c}[D_i\sigma_n + D_n\sigma_i]\rho_i^k\rho_n^k \\ & + \sum_{i=1}^{n_c}\left[\Gamma_i^n\rho_i^k - \frac{1}{2}\Gamma_n^i\rho_n^k\right] - \varepsilon_n\rho_n^k \\ & - \delta_{m,n}\sqrt{m^k}[\rho_m^k]^2\sum_{i=1}^{n_c} iD_i\rho_i^k - D_n\nabla^2\rho_n^k, \end{aligned} \quad (1)$$

where ρ_n^k and ρ_m^k are the two-dimensional (2D) densities of

subcritical mobile species of size n (monomers for $n = 1$ and clusters for $n > 1$) and of supercritical immobile species (islands), respectively, both belonging to the k-indexed ML (substrate, $k = 0$). The clusters are assumed to be 1 ML high with negligible step-edge barriers, i.e., no nucleation on their tops. Thus, clusters coarsen by both intralayer diffusion (at a rate D_n) and interlayer diffusion (instantaneous descent across the cluster edges). The coarsening clusters become islands when their size exceeds a critical size of $n_c = 7$. Interlayer mass exchange from the island tops is inhibited by strong step-edge barriers; hence the island tops serve as confined areas m^k (average island size) to nucleate $m^k\rho_n^{k+1}$ clusters and $m^k\rho_m^{k+1}$ islands belonging to upper $(k+1)^{\text{th}}$ ML. These constraints result in the formation of 3D mounds comprised of stacked MLs. The islands coarsen only by intralayer diffusion, which is comprised of both the capture of mobile species and island coalescence: $\partial m^k/\partial t \approx \sqrt{m^k}\sum_{i=1}^{n_c} iD_i\rho_i^k + \rho_m^k m^k\sqrt{m^k}\sum_{i=1}^{n_c} iD_i\rho_i^k$. The terms in Eq. (1) correspond to the following mechanisms. First term: The *random incidence* [$F = F(t)$ denotes the time-dependent flux of minority chemical species for a deposition rate $\tilde{F} \approx \int_{t=0}^{t=1s} F(t')\partial t'$]; and *transient mobility* [4] or *atomic insertion* of incident hyperthermal species (with $E^{\text{kin}} \sim$ 1–24 eV, Ref. [5]) from vapor [where $A_n = (\sqrt{n} + R/n)^2$, R being the incorporation radius] [3,4]. Second and third terms: *cluster coarsening* by random walk diffusion $\{D_n(m^k) \approx [D_n(m^k \to \infty)]^2/\min[D_n(m^k \to \infty), m^k\sqrt[3]{\ln(m^k)}]$ and $\sigma_n \propto \sqrt{n}$ are the diffusion coefficient in the island tops (confined regions) and coverage-independent capture number, respectively}. Fourth term: *cluster dissociation* (Γ_n^j, binary dissociation rate of an n-sized cluster into a pair of clusters of sizes j and $n - j$). Fifth to seventh terms: *cluster reevaporation* (ε_n, reevaporation rate); decay in ρ_m due to *island coalescence;* and the *coverage dependence of the capture numbers* through a uniform depletion model [3], respectively.

η-coupled systems of $n_c + 1$ partial differential equations ($\partial\rho_1^k/\partial t, \ldots, \partial\rho_m^k/\partial t$, $\partial m^k/\partial t$ with $k = 1, \ldots, \eta$) each in Eq. (1) were numerically solved using the *method of the lines* to discretize the 2D space, and then time integrated by the *Runge-Kutta method*. The considered initial (boundary) conditions were: $\rho_n^k(\vec{r}, t = 0) = 0$ [$\rho_n^1(\vec{r} \to \vec{r}_m, t) = 0$, where $\vec{r}_m$ indicates the positions of the $1/\sqrt{\rho_m^1}$-spaced islands acting as sink for mobile species]. To compute Eq. (1), the parameters for clusters of any size were estimated by applying empirical size-scaling relationships to reported values for monomers [3], which were taken within the typical range for highly corrugated oxide surfaces [6,7]. Once computed, $\rho_n^k(\vec{r}, t)$ was space averaged and its evolution together with that of $m^k(t)$ are the mean-field features used to describe the growth kinetics of: MBE (thermal continuous flux, $F(t) = \tilde{F}$ and $R = 0$), SP (hyperthermal continuous flux, $F(t) = \tilde{F}$ and $R > 0$), FE (thermal pulsed flux, $F(t) = \phi(t)\tilde{F}$ and $R = 0$) and PLD (hyperthermal pulsed flux, $F(t) = \phi(t)\tilde{F}$ and $R > 0$) with $\phi(t) = U(t_0 - \tau)/t_0\nu$. For pulsed fluxes, t_0 and ν are the pulse-width and repetition rate, respectively; $U(t_0 - \tau)$ is the unit-step function and τ denotes the time lapsed from the previous pulse. The resulting surfaces were investigate in regard to: (i) roughnesses $\omega(t) \approx \sqrt{\sum_{k=0}^{\eta}\{\theta^k - \theta^{k+1}\}[k - \int_0^t F(t)\partial t]^2}$ (where $\theta^k = \sum_{i=1}^{7} i\rho_i^k + m^k\rho_m^k$ denotes the fractional coverage of the k^{th} ML); (ii) number of uncovered [8] layers η [defined from $1 - \sum_{k=1}^{\eta}\theta^k/\int_0^t F(t)\partial t \le 10^{-2}$] that form the surface; and (iii) the average size of the species per ML $M^k = \theta^k/[\sum_{i=1}^{7}\rho_i^k + \rho_m^k]$.

Figure 1 shows the thickness evolution of the roughness during the early growth stage (up to a thickness [8] of 3 MLs, i.e., $d \le 0.8$ nm) for the four PVD techniques. The surfaces produced by the pulsed techniques (FE and PLD) were flatter than those obtained using the techniques with continuous fluxes (MBE and SP). In addition, an increase in E^{kin} of the incident species—from thermal (FE) to hyperthermal (PLD)—within the pulsed flux gave rise to a further decrease in roughness. These findings are consistent with experimental reports [9] indicating that PLD is the best PVD technique to prepare the flattest films. Note that to date, no conclusive insights into the origin of the lower roughness of PLD-grown films have been provided [9,10]. Conversely, continuous fluxes of hyperthermal species (SP) produce an extra increase in ω with respect to that obtained by MBE. Thus, the roughness of PVD-grown films as thin as $d = 3$ MLs in thickness can vary by 20%

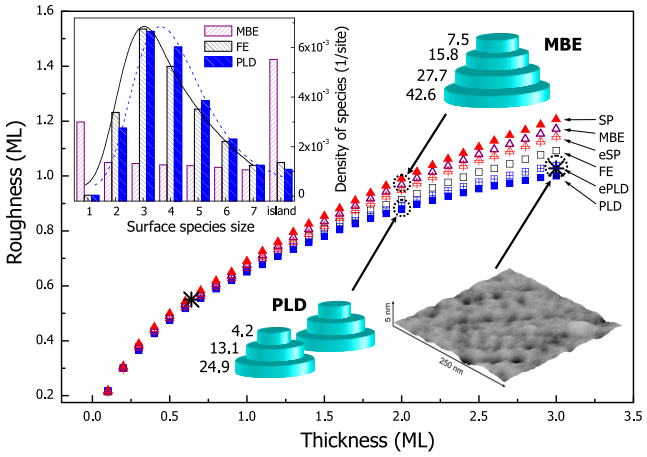

FIG. 1 (color online). Thickness dependence of the roughness for four distinctive PVD techniques: SP (▲), MBE (△), FE (□), and PLD (■); and their energetic counterparts eSP (crossed △) and ePLD (crossed □). Asterisks denote the data reported [11] for PLD-grown YSZ films/InP(100). AFM-imaged morphology of the $d = 3.0 \pm 0.1$-ML-thick YSZ film is shown [1-ML = 0.26 nm]. Sketches depict the morphology of the average mounds formed at $t = 20$ s by PLD and MBE. The numbers correspond to cross sections per ML and the amount of structures indicates the mound density ratio. Inset: Size distributions of the surface species generated at $t = 1$ s.

(from $\omega \approx 1$ to 1.2 MLs) depending on the growth kinetics. Representative morphologies of the 3D mounds formed at $t = 20$ s by PLD and MBE are sketched in Fig. 1. Previous statistical analysis showed [3] that the pulsed techniques produce high, nonequilibrium densities of moderate-sized clusters, which are small enough to prevent partially the nucleation of upper MLs prior to layer completion inducing a 2D growth habit. On the contrary, continuous fluxes produce large islands that give rise to well-shaped 3D mounds. The use of hyperthermal fluxes (SP and PLD) instead of thermal ones (MBE and FE) strengthens both opposite behaviors. The critical size $n_c = 7$ (described above) was chosen to get a good agreement (as shown in Fig. 1) between the ω evolution simulated for PLD kinetics and experimental data [11] for PLD-grown Y-stabilized ZrO_2 (YSZ) films on InP(100).

To account for the sensitivity of the roughness to the existence of a non-negligible fraction ($\alpha > 0$) of energetic incident species [5] ($E^{\mathrm{kin}} > 24$ eV)—able to break up surface clusters by direct impingement—in nonthermal fluxes, the first term in Eq. (1) was replaced with $m^{k-1}\rho_m^{k-1}F[\{1-\alpha\}A_{n-i}\rho_{n-1}^k - \{1-\alpha\}A_n\rho_n^k - X_n n\rho_n^k + X_{n+1}\{n+1\}\rho_{n+1}^k]$, where X_n describes the cluster breakup power of the flux [12]. The roughness computed for $X_n > 0$ [energetic SP (eSP) and PLD (ePLD)] is plotted in Fig. 1 to be compared with their hypertermal ($X_n \approx 0$ counterparts, SP and PLD). As shown, the cluster breakup phenomenon induces opposite effects on the roughness depending on the flux nature. Specifically, ω decreases for continuous fluxes (eSP) but increases for pulsed fluxes (ePLD). Whereas the decrease in the roughness under energetic continuous fluxes agrees with previous results [13], the increase in ω for pulsed fluxes disagrees with the existing models [14] that explained the low roughnesses obtained by PLD in terms of a "milling effect" of surface clusters and islands by energetic species in the ablation plume. In addition, these models [14] do not clarify the origin either of the low roughness obtained in oxide films grown by PLD [6,11] using moderate laser fluence ~3–5 J/cm^2 and high enough oxygen pressures (~10^{-3}–10^2 mbar) to thermalize the energetic species, which results in $\langle X_n \rangle \ll 1$ [12].

To get insights into the origin of the lower roughness achieved from pulsed fluxes, the size distribution and the coarsening kinetics of the surface species generated for fluxes of different natures were investigated. Figure 1 *inset* shows the size distributions of surface species after $t = 1$ s of growth. The continuous flux generates a bimodal size distribution with a large number of islands immersed in a background of small mobile species (mainly monomers), whereas the pulsed flux produces a unimodal distribution characterized by high densities of moderate-sized clusters (centered at $n = 3$–4) and a partial depletion of monomers [3]. Inspection of the maxima of the curves for pulsed fluxes reveals that the size distribution shifts to slightly larger cluster sizes as E^{kin} increases.

The scheme in Fig. 2 provides a comprehensive explanation for the above results. The roughness of an epitaxial film is mainly determined by the number η of uncovered MLs that form its surface; in general, ω rises as η increases. The nucleation of a new ML requires that the islands in the ML below are larger than the critical size $m^{k-1} > n_c \approx t_0\nu/\tilde{F}t^{\mathrm{res}}$ that is defined as the size at which the nucleation rate on the island is equal to the rate of escape ($\sim 1/t^{\mathrm{res}}$) from it. The residence time t^{res} spent by mobile species on an island is determined by the island-size dependence of the step-edge barrier which means that the ω evolution is closely related to the coarsening kinetics of the surface species evolving from clusters with negligible step-edge barriers ($t^{\mathrm{res}} \ll t_0$) to islands with strong barriers ($t_0 \ll t^{\mathrm{res}} \approx 1/\varepsilon_n$). On the basis of our results and the classic description of the growth for continuous fluxes, we propose a distinctive coarsening mechanism, namely, kinetically limited Ostwald ripening to account for the thickness dependence of ω in films grown from pulsed fluxes:

Continuous flux [Fig. 2(a)].—The coarsening occurs through the aggregation of small mobile species (mainly monomers) belonging to the background between islands. The background is continuously fed by the flux whose supersaturation $\psi_{\mathrm{cont.}} = \ln[\tilde{F}/p(T)]$, where $p(T)$ is the vapor pressure of the deposited material) produces a high density of monomers. This density ρ_1, which is higher than the equilibrium adatom densities for n-sized clusters

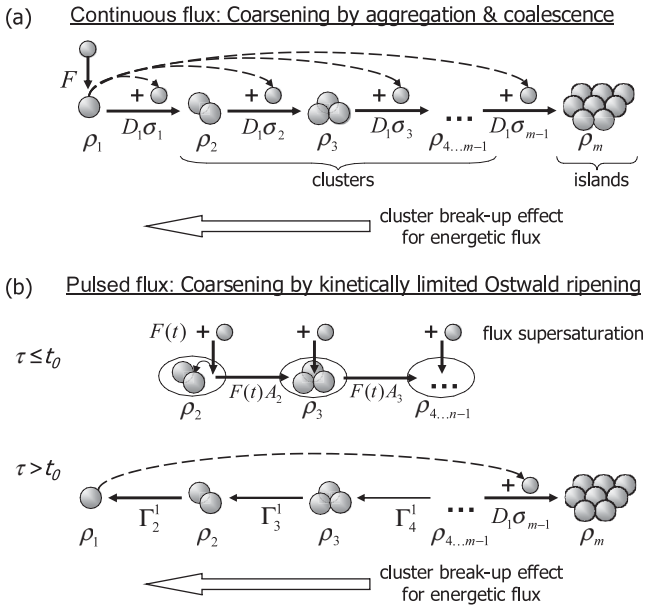

FIG. 2. Schematic representation of the coarsening mechanisms (solid arrows) for growth kinetics using nonenergetic continuous and pulsed fluxes. Dashed curves denote the capture of monomers from the background in (a) and from cluster dissociation in (b). Open arrows indicate the effect of the cluster breakup for energetic fluxes: arrows (solid and open) orientated in opposed directions (a) [in the same direction (b)] imply that the coarsening becomes slower (faster).

$\rho_1^e(n) \propto \rho_1^e(n \to \infty)[1 + 1/k_B T\sqrt{n}]$, stabilizes the clusters against dissociation. For hyperthermal fluxes [5] ($E^{\text{kin}} \sim$ 1–24 eV, e.g., growths in gas atmosphere) the coarsening proceeds more rapidly due to the transient mobility, which explains the high roughness of SP-grown films. Whereas for energetic fluxes [5] ($E^{\text{kin}} > 24$ eV, e.g., plasma-assisted growths in vacuum), by contrast, the coarsening is slower due to cluster breakup effects that reduce the roughness [13].

Pulsed flux [Fig. 2(b)].—Coarsening occurs via the dissociation of small species and the aggregation of the resulting monomers into larger clusters through an Ostwald ripening mechanism. The pulsed flux (as high as $10^3\tilde{F}$ for $t_0\nu \approx 10^{-3}$) is supersaturated with respect to the continuous flux ($\Delta\psi = \psi_{\text{pulsed}} - \psi_{\text{cont}} = -\ln[t_0\nu]$), which produces an extra drop in the condensation energy ($\Delta G = -k_B T\Delta\psi$). This gives rise (for $\tau \leq t_0$) to the abrupt formation of moderate-sized clusters and the partial depletion of monomers [3]. After the flux is stopped (for $\tau > t_0$), a further decay in ρ_1 occurs (due to aggregation to existing clusters) down to values lower than the equilibrium adatom density of the smallest clusters [initially dimers, $\rho_1 < \rho_1^e(n = 2)$], which then dissociate at a rate $\propto\Gamma_2^1$. The monomers resulting from dimer dissociation stabilize the larger clusters causing them to coarsen. Once the excess dimers are removed, the trimers become unstable and so on, i.e., as demonstrated in Ref. [3], it is only when the density of n-sized clusters tends to its equilibrium value that the $(n + 1)$-sized clusters become unstable with relaxation times $\propto(D_1/\Gamma_2^1)^n$, which become longer as the cluster sizes increase. This process allows larger clusters ($4 \leq n \leq n_c$) to be kinetically stable [3] between pulses, which leads to a slowing of the island coarsening. Consequently, the shift of the size distribution curve of the excess clusters to larger sizes (implying longer relaxation times) as E^{kin} of the incident species increases (Fig. 1, inset) accounts for the lowest PLD roughness. Conversely, breakup of the moderate-sized clusters by impinging energetic species [5] contributes to a shortening of the relaxation times of the excess clusters, and thus promotes rapid island coarsening. This explains the increase in ω for films grown using pulsed fluxes with a fraction of energetic species (ePLD). The fact that the growth kinetics of PLD is driven by kinetically limited Ostwald ripening is a ground-breaking finding. The omission of this information in previous models [10,14] has restricted their capability to address the existing data [6,9,11].

In conclusion, the study of four PVD techniques indicated that those based on pulsed fluxes of hyperthermal species (PLD in a gas atmosphere) are the best ones for preparing the flattest ultrathin films. The low roughnesses of the thus-grown films are due to coarsening by Ostwald ripening controlled by the slow dissociation kinetics of moderate-sized clusters. These clusters, which abruptly form at high densities in PLD-type growth kinetics, are small enough to prevent partially the nucleation of upper MLs previous to layer completion and large enough to be stable between flux pulses.

Work supported by Projects No. ESP2006-14282-C02-02, CCG06-UAM/MAT-0466 and the *Ramón y Cajal* program (MEC).

*enrique.vasco@icmm.csic.es

[1] S. S. P. Parkin, C. Kaiser, and A. Panchula *et al.*, Nat. Mater. **3**, 862 (2004); S. Yuasa, A. Fukushima, and H. Kubota *et al.*, Appl. Phys. Lett. **89**, 042505 (2006).

[2] J. B. Maxson, D. E. Savage, and F. Liu *et al.*, Phys. Rev. Lett. **85**, 2152 (2000).

[3] E. Vasco, New J. Phys. **8**, 253 (2006).

[4] E. Vasco and J. L. Sacedon, Phys. Rev. Lett. **98**, 036104 (2007).

[5] E^{kin} ranges describing the interaction of incident non-thermal species (here, atomic Zr and Y) with the matter (3-ML thick YSZ film/InP) [11] were estimated—(i) hyperthermal range ($E^{\text{kin}} \sim$ 1–24 eV) comprising transient mobility and atomic insertion, and (ii) energetic range that embraces the generation of surface adatom-vacancy pairs for $E^{\text{kin}} > 24$ eV—using the TRIM code by J. F. Ziegler *et al.*, *The Stopping and Range of Ions in Solids* (Pergamon, New York, 1985). See EPAPS Document No. E-PRLTAO-99-043750 for details. For more information on EPAPS, see http://www.aip.org/pubservs/epaps.html.

[6] B. Dam and B. Stauble-Pumpin, J. Mater. Sci.: Mater. Electron. **9**, 217 (1998).

[7] Simulation parameters: $\tilde{F} = 0.1$ ML/s; for pulsed fluxes, $t_0 = 1$ ms and $\nu = 1$ Hz; incorporation radius for thermal (hyperthermal) species $R = 0$ ($R = 1$); cluster-size dependent diffusion barrier $E^d(n) = E_1^d[1 + \{n - 1\}/10]$ (for monomers $E_1^d = 2.0$ eV); coordination-dependent binding energy [4] $E^b(n) = E_2^b[p(z) - 1/p(1) - 1]$ ($E_2^b = 0.60$ eV being the dimer binding energy); evaporation barrier $E_1^e =$ 2.5 eV and $k_B T = 75$ meV.

[8] Since specific mechanisms for ML completion (e.g., downhill funneling, step-edge barrier lowering at kink sites) were not considered, the longest simulation time was chosen to be shorter than the completion time of first ML for each PVD technique.

[9] H. Jenniches, M. Klaua, and H. Hoche *et al.*, Appl. Phys. Lett. **69**, 3339 (1996); B. Shin and M. J. Aziz, Phys. Rev. B **76**, 085431 (2007).

[10] B. Hinnemann, H. Hinrichsen, and D. E. Wolf, Phys. Rev. E **67**, 011602 (2003).

[11] E. Vasco and C. Zaldo, J. Phys. Condens. Matter **16**, 8201 (2004).

[12] See EPAPS Document No. E-PRLTAO-99-043750 for simulation parameters for energetic fluxes: $\alpha \approx 0.75$ and $\langle X_n \rangle \approx 0.3$. For more information on EPAPS, see http://www.aip.org/pubservs/epaps.html.

[13] J. M. Pomeroy, J. Jacobsen, and C. C. Hill *et al.*, Phys. Rev. B **66**, 235412 (2002).

[14] P. R. Willmott, R. Herger, and C. M. Schleputz *et al.*, Phys. Rev. Lett. **96**, 176102 (2006).